Are the Gas-Phase Structures of Molecular Elephants Enduring or				
Ephemeral? Results from Time-Dependent, Tandem Ion Mobility				
Benjamin P. Zercher, Seoyeon Hong, Addison E. Roush, Yuan Feng, Matthew F. Bush*				
Contribution from the:				
University of Washington, Department of Chemistry, Box 351700				
Seattle, WA 98195-1700				
*Email: mattbush@uw.edu				

## **Abstract**

The structural stability of biomolecules in the gas phase remains an important topic in mass spectrometry (MS) applications for structural biology. Here, we evaluate the kinetic stability of native-like protein ions using time-dependent, tandem ion mobility (IM). In these tandem IM experiments, ions of interest are mobility-selected after a first dimension of IM and trapped for up to ~14 seconds. Time-dependent, collision cross section distributions are then determined from separations in a second dimension of IM. In these experiments, monomeric protein ions exhibited structural changes specific to both protein and charge state, whereas large protein complexes did not undergo resolvable structural changes on the timescales of these experiments. We also performed energy-dependent experiments, i.e., collision-induced unfolding, as a comparison for time-dependent experiments to understand the extent of unfolding. Collision cross section values observed in energy-dependent experiments using high collision energies were significantly larger than those observed in time-dependent experiments, indicating that the structures observed in time-dependent experiments remain kinetically trapped and retain some memory of their solution-phase structure. Although structural evolution should be considered for highly charged, monomeric protein ions, these experiments demonstrate that higher-mass protein ions can have remarkable kinetic stability in the gas phase.

# Introduction

Native mass spectrometry (MS) has emerged as a useful addition to the structural biology toolkit, both as a standalone technique as well as through recent integration with high-resolution imaging. For example, MS can reduce sample heterogeneity in electron microscopy by massselecting and depositing ions from a native electrospray ion beam, enabling electron microscopy imaging of protein complexes.<sup>2,3</sup> Native electrospray beam deposition was also used to probe the flexibility of a monoclonal antibody with low-energy electron holography, a single-molecule imaging technique that requires ultrapure substrates.<sup>4</sup> Additionally, free-electron lasers probe solvent-free biomolecules;<sup>5</sup> an electrospray ionization source reduced nonvolatile contaminants to enable the analysis of 35-nm biomolecules, three orders of magnitude smaller than previously possible. Beyond imaging techniques, ion mobility (IM) is a gas-phase structural technique that has experienced increased adoption in recent years. <sup>7,8</sup> In IM, charged ions undergo collisions with a neutral background gas as they traverse a drift region under the influence of an applied electric field. The amount of time spent in the drift region is inversely proportional to the ion's mobility (K), from which a collision cross section ( $\Omega$ ) value can be determined. Results from IM-MS studies have been used to inform structural modeling, <sup>10–12</sup> characterize quaternary structure<sup>13,14</sup> and ligand-induced conformational changes, <sup>15,16</sup> and probe the transient species involved in protein-protein interactions and their folding intermediates. 17–19

To increase the utility of IM-MS, next-generation IM measurements aim to differentiate previously unresolved structures by leveraging high-resolution and multidimensional separations. The resolving power of a single conformation in IM can increase with the square root of the path length or separation time. For example, the Waters Cyclic IMS system can subject ions to an arbitrary number of passes through an off-axis ring to increase the path length

and thus the resolution of the separation.<sup>20</sup> Using multiple passes through a serpentine path,

Structures for Lossless Ion Manipulations (SLIM)<sup>21</sup> has achieved resolving powers of ~400-600

over a 679.5 m pathlength separation.<sup>22</sup> These instrument architectures can also enable IM-IM, or
tandem IM, in which two IM separations are separated by a mobility-dependent selection to
increase the selectivity of the measurement. Initially demonstrated on sequential, serial IM
components,<sup>23–25</sup> these new instrument geometries provide flexible tandem IM operation
modes.<sup>20,26</sup> Furthermore, both the Waters Cyclic IMS and the SLIM architecture have the
capability not only for IM-IM, but also for IM<sup>n</sup>, in which ions can be selected, activated, and
analyzed by subsequent dimensions of IM.

Although it is generally accepted that native-like ions can be generated from gentle ionization sources, <sup>27,28</sup> there has been a concerted experimental effort devoted to understanding the structural evolution of ions in the absence of solvent. IM-MS, <sup>28</sup> time-dependent IM-MS, <sup>29–31</sup> time-dependent IM-IM-MS, <sup>32–34</sup> molecular dynamics simulations, <sup>35–38</sup> electron capture dissociation, <sup>39,40</sup> and hydrogen-deuterium exchange <sup>41</sup> have been used to analyze the structures and stabilities of gas-phase ions. Relative to traditional, single-dimension IM, next-generation IM measurements require longer timescales, *e.g.*, hundreds of milliseconds and longer, <sup>42</sup> which provide additional opportunity for the properties of ions to change during measurements. Based on a meta-analysis, Breuker and McLafferty proposed a timeline for the gas-phase unfolding of protein ions where after initial desolvation events, side-chain collapse stabilizes the native-like structure before the loss of hydrophobic and electrostatic interactions result in structural rearrangements to lower-energy, gas-phase structures. <sup>43</sup> That analysis suggests that the timescales associated with next-generation IM separations may result in significant to total loss of native structure.

The objective of this study is to characterize the retention of native-like structures over a wide range of timescales to provide context for the information content of next-generation IM measurements. Here, we survey the gas-phase structural stabilities of a wide range of native-like protein ions using time-dependent, tandem IM measurements. Analytes ranged from small monomeric proteins to high-mass protein complexes. Apparent  $\Omega$  distributions of ions are monitored in time-dependent, tandem IM experiments to quantify how those distributions change with time. Complementary, energy-dependent experiments are used to understand potential unfolding pathways and the structural distributions of these ions at equilibrium.

## Methods

Sample Preparation and Ionization. Proteins were purchased from Sigma-Aldrich.

Native-like protein ions were generated using electrokinetic nanoelectrospray ionization<sup>44</sup> from 10 to 20 μM protein in aqueous 200 mM ammonium acetate adjusted to pH 7.0. IgG3 samples were also buffer exchanged using Micro Bio-Spin 6 columns (Bio-Rad, Hercules, CA) equilibrated with that same solution.

Time-dependent, Tandem IM. We have developed a flexible, modular instrument for IM-MS comprised of 12 modules,<sup>26</sup> as shown and described in Figure 1. The modules were constructed using the structures for lossless ion manipulations (SLIM) architecture; their use for native IM-MS has been described previously.<sup>26,32,45</sup> Ion packets are prepared for time-dependent, tandem IM experiments by diverting 12.5 ms of the incident ion beam to a junction trap at the end of the first module (<sup>1</sup>M). A junction trap is a potential well that confines ions when the input voltage of a board is biased relative to the output voltage of the preceding board.<sup>46</sup> The initial ion packet is released from the <sup>1</sup>M and is separated in the first dimension of IM (<sup>1</sup>D), which consists

of the <sup>2</sup>M through the middle of the <sup>7</sup>M. Voltage modulation at the intersecting paths of the <sup>7</sup>M is used to divert ions of interest to the orthogonal path for further analysis, whereas other ions continue to a collection electrode at the end of the collinear path of the <sup>7</sup>M. In these experiments, the timing of those voltages is used to isolate ions of a single charge state based on their mobility in the <sup>1</sup>D. Selected ions are then trapped at the interface between the <sup>7</sup>M and <sup>8</sup>M for variable delay times, defined as the amount of time between ion selection and the beginning of the second dimension of IM (<sup>2</sup>D).<sup>32</sup> After the delay time, ions are released from the junction trap by reducing the bias between the <sup>7</sup>M and <sup>8</sup>M. Ions are then separated along a path from the <sup>8</sup>M to the <sup>12</sup>M. In these experiments, the drift fields in the modules that comprise the <sup>1</sup>D were 4 V cm<sup>-1</sup>. The drift field in the orthogonal region connecting the <sup>7</sup>M and <sup>8</sup>M was 3.75 V cm<sup>-1</sup>, and the drift field in the  ${}^{2}D$  was 5 V cm ${}^{-1}$ . Drift fields were selected to optimize accuracy of  $\Omega$  measurements while reducing voltages of components relative to ground. In these experiments, the pusher of the time-of-flight mass analyzer was used as the master clock; delay times are the result of the timing of selection of specific precursor ions and its relation to a preset timing scheme used to manage digitizer memory. Additional information on the 12-module array, ion packet generation, and junction trapping conditions is provided in the Supporting Information.

Collision-Induced Unfolding (CIU). Energy-dependent experiments were conducted on a Waters Synapt G2 HDMS hybrid mass spectrometer (Waters Co., Wilmslow, UK) modified with an RF-confining drift cell containing nitrogen gas, as described previously.<sup>47</sup> CIU was monitored as a function of the voltage drop used to accelerate ions into the collision cell prior to IM separation.

Determining Apparent  $\Omega$  Distributions. Both experiments separate ions using electrostatic fields, not traveling waves, in nitrogen gas and data analysis is like that of drift

tubes. For time-dependent measurements, we derived a relationship between the applied drift field (E), the length of each region comprising the  $^2D$ , the observed arrival times, and K as described in the *Supporting Information*. Distributions of K were converted to apparent  $\Omega$  distributions using the Mason-Schamp equation. For CIU experiments, we used field-dependent measurements to convert arrival-times to apparent  $\Omega$  distributions as described previously. Median  $\Omega$  values,  $\widetilde{\Omega}$ , were determined from the cumulative distribution function of the apparent  $\Omega$  distributions.

Modeling of Observed Kinetics. To aid in the interpretation of time-dependent, tandem IM data, we developed a model that assumes that an initial population of structures (A) converts to a new population of structures (B) through first first-order kinetics. The model has three parameters, the  $\Omega$  of A ( $\Omega_A$ ),  $\Omega_B$ , and the rate constant. Based on those parameters, the model yields a weighted-average  $\Omega$  as a function of time. Using the Levenberg–Marquardt algorithm, we optimized the values of three parameters to minimize the least-squares difference between the modeled, weighted-average  $\Omega$  and the observed  $\widetilde{\Omega}$  as a function of time. The standard deviation of each parameter was estimated from the diagonals of the covariance matrix generated during optimization. This modeling was implemented using Python with the numpy<sup>49</sup> and astropy<sup>50</sup> libraries.

## **Results and Discussion**

Current- and next-generation IM measurements access a wide range of timescales (e.g.,  $10^{-3}$  to  $10^{1}$  s). Therefore, it is increasingly important to understand the extent to which the structures of native-like ions evolve over these time scales. To this end, we used time-dependent, tandem IM to survey the gas-phase stabilities of a range of native-like ions. These analytes were

selected to encompass a broad range of masses and collision cross sections ( $\Omega$ ) as shown in Figure 2. We first present the results from time- and energy-dependent experiments, and then compare those results. To provide additional context for the time-dependent results, we report results from a kinetic model, compare those results to other rates/timescales reported previously, and discuss their broader implications.

Time-Dependent Analysis of Native-Like, Monomeric Protein Ions. Native-like ions of 5+ and 6+ ubiquitin, 4+ insulin, 7+ cytochrome c, and 8+  $\beta$ -lactoglobulin were subjected to timedependent, tandem IM experiments. Those results are shown in the positive intensity traces in Figure 3; the corresponding negative intensity traces are for complementary energy-dependent experiments that will be the focus of the next section. In time-dependent experiments, ions are separated in the first dimension of IM (<sup>1</sup>D, Figure 1). Ions with the charge states of interest are selected at the seventh module (<sup>7</sup>M) and trapped at the interface between the <sup>7</sup>M and <sup>8</sup>M as a function of time prior to release into the second dimension of IM (<sup>2</sup>D). The effective temperatures of the trapped ions are estimated to be near, albeit somewhat above ambient temperature; the methodology<sup>51</sup> and results of those estimates are discussed in the *Supporting Information*. The delay time describes the time between selection and <sup>2</sup>D analysis. <sup>32</sup> For monomeric proteins, the longest delay times ranged from ~9-14 s. Maximum delay times were limited both by charge-transfer reactions that depleted the precursor ions, as well as nonspecific adduction that increased the mass of the selected ions and degraded the signal-to-noise ratio. Median  $\Omega$  values,  $\widetilde{\Omega}$ , were determined from the cumulative distribution function of the apparent  $\Omega$  distributions. Relative to mean  $\Omega$  values, we find that  $\widetilde{\Omega}$  values are less sensitive to outliers (e.g., low-intensity noise in the arrival-time distribution that is distal to the predominant feature) and can be determined robustly with less analyst supervision. The  $\widetilde{\Omega}$  extracted from the ion

populations with the shortest delay times agree with  $\Omega$  values reported previously for native-like ions, <sup>47,52</sup> indicating that the initial populations in these experiments maintain compact, native-like structures (see *Supporting Information*). Technical replicates of time-dependent experiments taken across multiple days show that these results are highly reproducible (Figure S2).

Three of the five monomeric analytes exhibit evidence for structural changes in these time-dependent experiments, *i.e.*, the apparent  $\Omega$  distributions depended on the delay time. Figure 3A shows results for 6+ ubiquitin. At the shortest delay time, the initial ion population exhibits a compact population centered near 12.5 nm², as well as the presence of a small shoulder resulting from ions with larger  $\Omega$  values. With increasing delay time, the compact population is depleted in favor of an extended population that exhibits a maximum  $\Omega$  above 14 nm². After ~9 s of trapping, the extended population is predominant. The structural transition for 6+ ubiquitin appears to be a discrete transition between two structures that are well resolved in the ²D. The magnitude of this increase in  $\Omega$  is consistent with experimental observations of a semi-folded state of 6+ ubiquitin, which has been attributed to a "solution-like conformer" based on results from long timescale (1 µs), mobile-proton, molecular dynamics simulations. Figure S3 shows representative mass spectra from these time-dependent experiments. These spectra exhibit evidence for both charge transfer to and complexation with molecules in the instrument, but no evidence for fragmentation.

Other monomeric proteins underwent more subtle structural changes. Figure 3B shows that the time-dependent apparent  $\Omega$  distributions of 5+ ubiquitin shift monotonically towards larger  $\widetilde{\Omega}$  with increasing delay time. The initial population exhibits a  $\widetilde{\Omega}$  of 12.0 nm<sup>2</sup>; after ~14 seconds of trapping in the gas-phase, that value increases to 12.3 nm<sup>2</sup>. The apparent  $\Omega$  distributions of 7+ cytochrome c also exhibit subtle changes with increasing delay times (Figure

3C). The  $\widetilde{\Omega}$  of the initial ion population is 15.7 nm², and increases to 16.6 nm² after ~14 s of trapping. These results for 7+ cytochrome c are consistent with previous data acquired in analogous experiments performed using a 6-module array. <sup>32</sup> Both 5+ ubiquitin and 7+ cytochrome c appear to evolve through a continuum of conformations or perhaps a small number of conformers that are not resolved in these IM experiments. Figure 3D shows that the initial ion population for 8+  $\beta$ -lactoglobulin exhibits a  $\widetilde{\Omega}$  of 20.5 nm² and that the apparent  $\Omega$  distributions appear to be largely independent of the delay time, even after 4 s. 4+ insulin (Figure S1) also did not undergo any significant changes in mobility as a function of delay time.

These time-dependent, tandem IM experiments show that the magnitude and timescales of the structural changes for these native-like, monomeric protein ions depend on the identity and charge state of the ion. To evaluate the magnitude of these changes, we will characterize these same ions using energy-dependent IM experiments and then compare the results from the time-and energy-dependent experiments.

Energy-Dependent Analysis of Native-Like, Monomeric Protein Ions. Collision-induced unfolding (CIU) probes the structures of ions as a function of the energy deposited through collisional activation prior to IM analysis. <sup>53,54</sup> Activated ions can overcome isomerization barriers to form additional structures that appear to be kinetically stable for at least milliseconds. <sup>54</sup> Here, we will use CIU to characterize the same protein ions that were analyzed using time-dependent experiments, which did not include intentional collisional activation.

The apparent  $\Omega$  distributions generated from CIU experiments are shown in negative, normalized intensities in Figure 3. Figure 3A shows that at the lowest-energy, 6+ ubiquitin exhibits a bimodal distribution with a more-compact population near 12.5 nm<sup>2</sup> and more-extended population centered near 14 nm<sup>2</sup>. With increasing energy, the compact population is

depleted in favor of more extended population centered near 15 nm<sup>2</sup>. Finally, as the laboratory-frame energy is increased above 96 eV, the population centered near 15 nm<sup>2</sup> is depleted in favor of that centered near 18 nm<sup>2</sup>. That distribution centered near 18 nm<sup>2</sup> persists with increasing energy until fragmentation occurs. The persistence of that distribution suggests those ions populated the gas-phase equilibrium (or quasi-equilibrium)<sup>55</sup> distribution of structures.

For 5+ ubiquitin and 7+ cytochrome c, the apparent  $\Omega$  distributions widen and shift towards higher  $\Omega$  values with increasing energy. For 5+ ubiquitin, the initial ion population is centered near 12 nm², whereas the most extended population is centered between 13 and 14 nm². For 7+ cytochrome c, the initial ion population observed near 16 nm² is depleted in favor of a distribution centered near 22 nm². For 8+  $\beta$ -lactoglobulin, the initial population was centered near 21 nm². The initial changes with increasing energy are small, but for laboratory-frame energies above 100 eV, much larger structures were observed. At the highest energies, a wide distribution was observed with a  $\widetilde{\Omega}$  near 26 nm² and a maximum value near almost 28 nm². Whereas all other monomeric ions underwent structural evolution in these energy-dependent experiments, the apparent  $\Omega$  distributions of 4+ insulin appears to be independent of energy (Figure S1).

Native-Like, Monomeric Protein Ions Can Retain Memories of their Original Structures for Many Seconds in the Gas Phase. The apparent  $\Omega$  distributions from time-dependent experiments can be compared to those from energy-dependent experiments to provide context for the structural transitions observed in absence of intentional collisional activation. The change in  $\widetilde{\Omega}$  is quantified by:

$$Relative \Omega = \frac{\tilde{\Omega}_{final}}{\tilde{\Omega}_{initial}} \tag{1}$$

where "initial" describes the ion population that experienced the shortest delay time or the lowest laboratory-frame energies and "final" describes the ion population that experienced the longest delay time or the highest laboratory-frame energies.

Figure 4 shows the relative  $\Omega$  values from time-dependent and energy-dependent experiments for each of the monomeric proteins analyzed. Energy-dependent experiments resulted in relative  $\Omega$  values of 100%, 110%, 127%, 134%, and 136% for 4+ insulin, 5+ ubiquitin,  $8+\beta$ -lactoglobulin, 7+ cytochrome c, and 6+ ubiquitin respectively. These same protein ions exhibited relative  $\Omega$  values of 100%, 102%, 101%, 105%, and 114% in timedependent experiments. 4+ insulin was the only monomeric protein that did not exhibit any change during these experiments (Figure S1). This ion may adopt a stable distribution of structures prior to analysis, or alternatively, the changes that do occur do not affect the mobility of the ions. As no changes in mobility are observed in energy-dependent experiments, 4+ insulin serves as a negative control for time-dependent experiments. For the other monomeric protein ions, energy-dependent experiments yield a greater increase in  $\Omega$  than the corresponding timedependent experiments. For example, 8+ β-lactoglobulin did not exhibit resolvable structural changes in time-dependent experiments but exhibited significant unfolding in energy-dependent experiments (Figure 3D). 6+ ubiquitin underwent a single discrete transition in time-dependent experiments, and then exhibited evidence for the formation of an even larger, gas-phase annealed structure in energy-dependent experiments (Figure 3A).

The large increases in apparent  $\Omega$  observed in these energy-dependent experiments are consistent with increases in drift time reported in CIU experiments in the literature.<sup>31</sup> Since the ions at the highest energies in the CIU experiments exhibited similar apparent  $\Omega$  distributions over a wide range of energies, that suggests that a gas-phase equilibrium (or quasi-equilibrium)<sup>55</sup>

distribution of structures was adopted in those experiments. Therefore, the  $\widetilde{\Omega}_{final}$  values for the CIU experiments represent an upper limit; smaller  $\widetilde{\Omega}_{final}$  values for the time-dependent experiments indicates that structures remain kinetically trapped and retain some memory of their original structures. From these results, it can be shown that native-like protein ions undergo time-dependent structural changes that are specific to both protein and charge state. However, the observable structural changes do not appear to correlate to a full rearrangement to the larger, gas-phase structures formed in energy-dependent experiments. Although the structural evolutions observed in our time-dependent experiments are significant and have implications for IM measurements of native-like ions, the small magnitude of those changes relative to the low-energy, gas-phase annealed structures points to a remarkably long memory of the native-like fold in the gas phase.

Native-Like Ions of Protein Complexes Appear to Have Mobilities that are Independent of Time for at Least a Second in the Gas Phase. Using time-dependent, tandem IM, we also characterized the gas-phase stabilities of 16+ avidin, 21+ concanavalin A, and 25+ IgG3. Avidin and concanavalin A are noncovalently bound homotetramers. IgG3 is comprised of two heavy and two light chains that are connected through covalent and noncovalent interactions; the gas-phase structures and dynamics of antibodies like IgG3 are of particular interest because of the potential applications of IM-MS in the development and characterization of biopharmaceuticals.  $^{37,56,57}$  The apparent  $\Omega$  distributions of these ions are shown in Figure 5 for delay times up to  $\sim$ 2 s. Whereas the distributions for most monomeric proteins exhibited some degree of change as a function of time (Figure 3), the distributions for these larger native-like ions appear to be essentially independent of time. The apparent  $\Omega$  distributions remain well overlaid and  $\widetilde{\Omega}$  vary by less than 1%, even after more than 1 s in the gas phase.

One possibility for the lack in change of  $\Omega$  is that the ions probed in these experiments have already adopted gas-phase, equilibrium structures, rather than kinetically trapped, nativelike structures. To determine whether the ions probed in this experiment are native-like, observed  $\widetilde{\Omega}_{initial}$  values can be compared to previous  $\Omega$  measurements of native-like ions. The  $\widetilde{\Omega}_{initial}$ values observed in these experiments are 41.9, 61.3, and 75.5 nm<sup>2</sup> for 16+ avidin, 21+ concanavalin A, and 25+ IgG3, respectively. For avidin and concanavalin A, observed  $\tilde{\Omega}_{initial}$ values are within 1% of reported native-like  $\Omega$  values measured on an RF-confining drift cell,<sup>52</sup> whereas the observed  $\widetilde{\Omega}_{initial}$  value for 25+ IgG3 agrees well with previous measurements that used traveling-wave IM.<sup>58</sup> Furthermore, these proteins have been characterized previously using CIU experiments and those studies reported significant increases in  $\Omega$  with increasing energy.  $^{53,57,59}$  For example, 16+ avidin exhibited a  $\sim$ 42% increase in  $\widetilde{\Omega}$  with increasing energy.  $^{48}$ With increasing energy, four distinct gas-phase populations with significantly different drift times were observed for 15+ avidin and 19+ concanavalin A.53 CIU of antibodies also results in the appearance of multiple extended populations, with IgG3 exhibiting a ~45% increase in arrival time for its most extended population. <sup>57,59</sup> If the ions probed in these experiments had already adopted their global-minimum structures, observed  $\widetilde{\Omega}_{initial}$  values would differ greatly from previous measurements.

Although it is possible that these protein complexes undergo small rearrangements on these timescales that do not affect the measured mobility, the well-overlaid apparent  $\Omega$  distributions observed in these time-dependent experiments are evidence that these large, native-like protein ions do not undergo significant structural changes in the gas-phase at near ambient temperatures for >1 s. It follows that kinetic stability in the gas phase likely increases with mass or m/z, consistent with enhanced charge solvation in the structures of larger multimeric protein

ions (as well as the largest monomeric protein ion studied,  $\beta$ -lactoglobulin) than their smaller, monomeric counterparts. Note that the rates for both charge transfer to and complexation with other molecules appear to be greater for larger protein ions than for smaller protein ions (Figure S3). This is tentatively attributed to the larger  $\Omega$  values (Figure 2) and collision frequency of the former, but further characterization of these processes will be the subject of further investigation.

Kinetics of Structural Transitions and Comparison with Previous Experiments. Relative  $\Omega$  values are shown as a function of delay time in Figure 6 and reveal the stark contrast between the ions characterized in this study. Monomeric protein ions exhibit varied gas-phase stabilities, and analytes that undergo structural evolution exhibit the greatest change in apparent  $\Omega$  at the shortest delay times (Figure 6A). Conversely, the native-like structures of each of the multimeric protein ions, which also have significantly higher masses, are kinetically stable for seconds in the gas phase (Figure 6B). To quantify these time-dependent changes in structure, we modeled the experimental data assuming that an initial population of structures (A) converts to a new population of structures (B) through first first-order kinetics. We parameterized this model, which depends on the  $\Omega$  of A ( $\Omega_A$ ),  $\Omega_B$ , and the rate constant, to reproduce the experimental  $\widetilde{\Omega}$  determined as a function of delay time.

The results from this modeling are shown in Figure 6A and Table 1. This process yielded a rate constant of  $0.28\pm0.07~\rm s^{-1}$  (interval spans  $\pm$  one standard deviation) for 7+ cytochrome c, which is similar to the initial depletion rate  $(0.31\pm0.06~\rm s^{-1}, 90\%$  confidence interval) determined using analogous experiments performed using a 6-module array.<sup>32</sup> Note that the latter rate is based on a single-parameter model (the rate constant) of the depletion of the population of ions with apparent  $\Omega$  values between 14.14 and 16.32 nm<sup>2</sup> and for delay times ranging from 16 to 911 ms. Results for delay times ranging from 2031 to 33 231 ms were analyzed separately and

suggested a slower rate constant of  $(0.042\pm0.006~\text{s}^{-1}, 90\%$  confidence interval).<sup>32</sup> There was no clear evidence for slower kinetics at longer delay times in the present study, which may be attributable to differences in kinetic modelling or the range of delay times (up to 14 342 ms). Although no rate constant was reported, 7+ cytochrome c ions trapped in a cyclic IMS system underwent structural changes of a similar magnitude over several hundred milliseconds.<sup>31</sup> In earlier investigations, the compact population of 7+ cytochrome c ions stored in a Paul trap exhibited a depletion rate of  $40~\text{s}^{-1}$ , <sup>29</sup> which is significantly faster than the recent studies. This was attributed to possible differences in effective temperatures of ions between the experiments, <sup>32</sup> as well as differences in the solutions from which ions were generated.<sup>32</sup> Despite differences in rate constants, all studies observed time-dependent structural changes for 7+ cytochrome c.

This analysis yields rate constants for 5+ and 6+ ubiquitin of  $0.91\pm0.20$  and  $0.84\pm0.05$  s<sup>-1</sup>, respectively, which are similar to each other and much faster than that for 7+ cytochrome c. Over the full range of delay times, 6+ ubiquitin exhibits a relative  $\Omega$  of 114%, whereas 5+ ubiquitin and 7+ cytochrome c exhibit much smaller relative  $\Omega$  of 102% and 105%, respectively (Figure 4). An intriguing, albeit speculative, possibility is that the unfolding of the initial 5+ and 6+ ubiquitin ions proceeds through similar transition states, but after those transition states, 6+ ubiquitin adopts a population of structures that has a much larger  $\Omega$  than 5+ ubiquitin. These results suggest that the rates of change and the magnitude of change in  $\Omega$  that occurs with increasing time are not necessarily correlated and highlight the need for future time-dependent experiments that more generally characterize the effects of charge state.

Notes that this isomerization rate for 6+ ubiquitin generated from native-like conditions  $(0.84 \pm 0.05)$  is greater than that reported for 6+ ubiquitin generated from a solution of 49:49:2 by volume water:methanol:acetic acid  $(0.2 \text{ s}^{-1})$ .<sup>30</sup> Due to differences in the experiments, it is

challenging to directly compare these results (see Figure S4 and associated discussion in the Supporting Information) and we were unable to identify a single, compelling origin for the difference in rate constants. This comparison highlights the need for future time-dependent experiments that directly characterize the effects of original solution conditions.

Because none of the larger protein ions appeared to convert to populations with larger  $\Omega$  values, we instead estimated the upper limit of the depletion rate constant for the initial population in time-dependent experiments. We estimated the  $\widetilde{\Omega}$  for the equilibrium conformation of 16+ avidin (50 nm²) based on previous energy-dependent experiments. Assuming first-order kinetics, we estimated the relative  $\widetilde{\Omega}$  that would be expected for selected rate constants (transparent lines, Figure 6B). This analysis shows that  $0.05~\text{s}^{-1}$  represents a conservative upper limit for the depletion rate of the initial population of 16+ avidin (Figure 6). This approach provides quantitative evidence that the multimeric protein ions probed in this study can retain elements of native-like structure at ambient temperature even over the longest timescales envisioned for next-generation IM and other native MS-enabled structural biology techniques.

# **Conclusions**

We surveyed the gas-phase structural stabilities of a wide range of native-like protein ions using time-dependent, tandem IM measurements on a modular instrument (Figure 1). Monomeric proteins exhibited a range of gas-phase stabilities, with three of the five analytes undergoing expansion to larger  $\widetilde{\Omega}$  on the millisecond to second timescale (Figure 3, positive intensity traces). The monomeric protein ions exhibited structural changes in time-dependent experiments at long times that were smaller than those observed in energy-dependent experiments at high energies (Figure 4), which indicates that these ions retain significant

memory of their solution-phase structure even after up to ~14 s in the gas phase. Whereas smaller, monomeric proteins exhibited varied gas-phase stabilities, the  $\Omega$  distributions of highermass, higher-m/z protein ions appeared to be independent of the delay times used in these experiments (Figure 5). We modeled the kinetics of the observed structural transitions (Figure 6) and compared rates of conversion with those reported in the literature.

These results provide context for future multidimensional IM experiments. For example, the apparent  $\Omega$  distributions of 6+ ubiquitin exhibit features for two populations, whose relative abundance would change on the timescale of many experiments. The apparent  $\Omega$  distributions of 5+ ubiquitin and 7+ cytochrome c exhibit comparatively subtle changes with increasing time, but the nature of the changes would be extremely challenging to identify and characterize using single-dimension IM experiments with long timescales. Although traditional IM-MS measurements have failed to differentiate closely related mAbs,  $^{57}$  our findings suggest that those structures are kinetically stable in the gas phase and may be amenable to high-resolution and multidimensional IM experiments that typically manipulate gas-phase ions for many tens to hundreds of milliseconds before detection.  $^{42}$ 

Based on a meta-analysis of results from a variety of experimental and computational studies, Breuker and McLafferty proposed that most noncovalent interactions present in native biomolecules would be lost in subsecond timescales and that new gas-phase structures would be predominate in the second to minute timescales. Although those predictions may be true for the highly-charged, monomeric protein ions that formed the basis of that meta-analysis, the present studies show that protein ions with larger m/z values and sizes (Figure 2) can have remarkable stabilities that kinetically trap elements of their original structures for seconds in the gas phase. These trends suggest that higher-m/z ions provide better solvation for excess charges and have

higher isomerization barriers. With these considerations in mind, the structural evolution of higher-mass protein ions likely occurs on the longer end of the timescales proposed by Breuker and McLafferty. We note that these conclusions are based on results from experiments that were performed using devices that have been optimized to minimize ion activation; 26,45,32 e.g., we estimate that the trapped ions in these experiments have effective temperatures that are near ambient (Table S1). Ions in other experiments may experience higher effective temperatures, 60–62 and with increasing effective temperature, we would predict more rapid depletion of the initial, most-native-like conformations. More generally, these results support the expanded use of next-generation IM experiments in structural MS by providing a framework for designing and interpreting the results of experiments with longer timescales.

**Supporting Information.** Supporting Information associated with this article includes Additional Methods, Effective Temperatures, Representative IM and MS data, and Comparisons with Prior Study of 6+ Ubiquitin from Denaturing Conditions.

Acknowledgments. This material is based upon work supported by the National Institute of General Medical Sciences of the National Institutes of Health through award R01GM130708 (M.F.B.), the National Science Foundation through award 1807382 (M.F.B.) from the Division of Chemistry, with partial co-funding from the Division of Molecular and Cellular Biosciences, and the National Science Foundation through award 2140004 (A.E.R.) from the Division of Graduate Education.

# References

- (1) Liko, I.; Allison, T. M.; Hopper, J. T.; Robinson, C. V. Mass Spectrometry Guided Structural Biology. Curr. Opin. Struct. Biol. 2016, 40, 136–144. https://doi.org/10.1016/j.sbi.2016.09.008.
- (2) Esser, T. K.; Böhning, J.; Fremdling, P.; Agasid, M. T.; Costin, A.; Fort, K.; Konijnenberg, A.; Gilbert, J. D.; Bahm, A.; Makarov, A.; Robinson, C. V.; Benesch, J. L. P.; Baker, L.; Bharat, T. A. M.; Gault, J.; Rauschenbach, S. Mass-Selective and Ice-Free Electron Cryomicroscopy Protein Sample Preparation via Native Electrospray Ion-Beam Deposition. *PNAS Nexus* 2022, 1 (4), pgac153. https://doi.org/10.1093/pnasnexus/pgac153.
- (3) Westphall, M. S.; Lee, K. W.; Salome, A. Z.; Lodge, J. M.; Grant, T.; Coon, J. J. Three-Dimensional Structure Determination of Protein Complexes Using Matrix-Landing Mass Spectrometry. *Nat. Commun.* **2022**, *13* (1), 2276. https://doi.org/10.1038/s41467-022-29964-4.
- (4) Ochner, H.; Szilagyi, S.; Abb, S.; Gault, J.; Robinson, C. V.; Malavolti, L.; Rauschenbach, S.; Kern, K. Low-Energy Electron Holography Imaging of Conformational Variability of Single-Antibody Molecules from Electrospray Ion Beam Deposition. *Proc. Natl. Acad. Sci.* 2021, 118 (51), e2112651118. https://doi.org/10.1073/pnas.2112651118.
- (5) Hajdu, J. Single-Molecule X-Ray Diffraction. Curr. Opin. Struct. Biol. 2000, 10 (5), 569–573. https://doi.org/10.1016/S0959-440X(00)00133-0.
- (6) Bielecki, J.; Hantke, M. F.; Daurer, B. J.; Reddy, H. K. N.; Hasse, D.; Larsson, D. S. D.; Gunn, L. H.; Svenda, M.; Munke, A.; Sellberg, J. A.; Flueckiger, L.; Pietrini, A.; Nettelblad, C.; Lundholm, I.; Carlsson, G.; Okamoto, K.; Timneanu, N.; Westphal, D.; Kulyk, O.; Higashiura, A.; van der Schot, G.; Loh, N.-T. D.; Wysong, T. E.; Bostedt, C.;

- Gorkhover, T.; Iwan, B.; Seibert, M. M.; Osipov, T.; Walter, P.; Hart, P.; Bucher, M.; Ulmer, A.; Ray, D.; Carini, G.; Ferguson, K. R.; Andersson, I.; Andreasson, J.; Hajdu, J.; Maia, F. R. N. C. Electrospray Sample Injection for Single-Particle Imaging with x-Ray Lasers. *Sci. Adv.* **2019**, *5* (5), eaav8801. https://doi.org/10.1126/sciadv.aav8801.
- (7) Lanucara, F.; Holman, S. W.; Gray, C. J.; Eyers, C. E. The Power of Ion Mobility-Mass Spectrometry for Structural Characterization and the Study of Conformational Dynamics.

  Nat. Chem. 2014, 6 (4), 281–294. https://doi.org/10.1038/nchem.1889.
- (8) Ben-Nissan, G.; Sharon, M. The Application of Ion-Mobility Mass Spectrometry for Structure/Function Investigation of Protein Complexes. *Curr. Opin. Chem. Biol.* 2018, 42, 25–33. https://doi.org/10.1016/j.cbpa.2017.10.026.
- (9) Gabelica, V.; Shvartsburg, A. A.; Afonso, C.; Barran, P.; Benesch, J. L. P.; Bleiholder, C.; Bowers, M. T.; Bilbao, A.; Bush, M. F.; Campbell, J. L.; Campuzano, I. D. G.; Causon, T.; Clowers, B. H.; Creaser, C. S.; De Pauw, E.; Far, J.; Fernandez-Lima, F.; Fjeldsted, J. C.; Giles, K.; Groessl, M.; Hogan, C. J.; Hann, S.; Kim, H. I.; Kurulugama, R. T.; May, J. C.; McLean, J. A.; Pagel, K.; Richardson, K.; Ridgeway, M. E.; Rosu, F.; Sobott, F.; Thalassinos, K.; Valentine, S. J.; Wyttenbach, T. Recommendations for Reporting Ion Mobility Mass Spectrometry Measurements. *Mass Spectrom. Rev.* 2019, *38* (3), 291–320. https://doi.org/10.1002/mas.21585.
- (10) Politis, A.; Park, A. Y.; Hyung, S.-J.; Barsky, D.; Ruotolo, B. T.; Robinson, C. V. Integrating Ion Mobility Mass Spectrometry with Molecular Modelling to Determine the Architecture of Multiprotein Complexes. *PLoS ONE* **2010**, *5* (8), e12080. https://doi.org/10.1371/journal.pone.0012080.

- (11) Thalassinos, K.; Pandurangan, A. P.; Xu, M.; Alber, F.; Topf, M. Conformational States of Macromolecular Assemblies Explored by Integrative Structure Calculation. *Structure* 2013, 21 (9), 1500–1508. https://doi.org/10.1016/j.str.2013.08.006.
- (12) Eschweiler, J. D.; Frank, A. T.; Ruotolo, B. T. Coming to Grips with Ambiguity: Ion Mobility-Mass Spectrometry for Protein Quaternary Structure Assignment. J. Am. Soc. Mass Spectrom. 2017, 28 (10), 1991–2000. https://doi.org/10.1007/s13361-017-1757-1.
- (13) Uetrecht, C.; Versluis, C.; Watts, N. R.; Wingfield, P. T.; Steven, A. C.; Heck, A. J. R. Stability and Shape of Hepatitis B Virus Capsids In Vacuo. *Angew. Chem. Int. Ed.* **2008**, 47 (33), 6247–6251. https://doi.org/10.1002/anie.200802410.
- (14) Marcoux, J.; Politis, A.; Rinehart, D.; Marshall, D. P.; Wallace, M. I.; Tamm, L. K.; Robinson, C. V. Mass Spectrometry Defines the C-Terminal Dimerization Domain and Enables Modeling of the Structure of Full-Length OmpA. *Structure* 2014, 22 (5), 781–790. https://doi.org/10.1016/j.str.2014.03.004.
- (15) Pacholarz, K. J.; Burnley, R. J.; Jowitt, T. A.; Ordsmith, V.; Pisco, J. P.; Porrini, M.; Larrouy-Maumus, G.; Garlish, R. A.; Taylor, R. J.; de Carvalho, L. P. S.; Barran, P. E. Hybrid Mass Spectrometry Approaches to Determine How L-Histidine Feedback Regulates the Enzyzme MtATP-Phosphoribosyltransferase. *Structure* 2017, 25 (5), 730-738.e4. https://doi.org/10.1016/j.str.2017.03.005.
- (16) Lai, A. L.; Clerico, E. M.; Blackburn, M. E.; Patel, N. A.; Robinson, C. V.; Borbat, P. P.; Freed, J. H.; Gierasch, L. M. Key Features of an Hsp70 Chaperone Allosteric Landscape Revealed by Ion-Mobility Native Mass Spectrometry and Double Electron-Electron Resonance. *J. Biol. Chem.* 2017, 292 (21), 8773–8785.
  https://doi.org/10.1074/jbc.M116.770404.

- (17) Smith, D. P.; Giles, K.; Bateman, R. H.; Radford, S. E.; Ashcroft, A. E. Monitoring Copopulated Conformational States during Protein Folding Events Using Electrospray Ionization-Ion Mobility Spectrometry-Mass Spectrometry. *J. Am. Soc. Mass Spectrom.* 2007, 18 (12), 2180–2190. https://doi.org/10.1016/j.jasms.2007.09.017.
- (18) Dupuis, N. F.; Wu, C.; Shea, J.-E.; Bowers, M. T. Human Islet Amyloid Polypeptide Monomers Form Ordered β-Hairpins: A Possible Direct Amyloidogenic Precursor. *J. Am. Chem. Soc.* 2009, 131 (51), 18283–18292. https://doi.org/10.1021/ja903814q.
- (19) Österlund, N.; Moons, R.; Ilag, L. L.; Sobott, F.; Gräslund, A. Native Ion Mobility-Mass Spectrometry Reveals the Formation of β-Barrel Shaped Amyloid-β Hexamers in a Membrane-Mimicking Environment. *J. Am. Chem. Soc.* **2019**, *141* (26), 10440–10450. https://doi.org/10.1021/jacs.9b04596.
- (20) Giles, K.; Ujma, J.; Wildgoose, J.; Pringle, S.; Richardson, K.; Langridge, D.; Green, M. A Cyclic Ion Mobility-Mass Spectrometry System. *Anal. Chem.* **2019**, *91* (13), 8564–8573. https://doi.org/10.1021/acs.analchem.9b01838.
- (21) Deng, L.; Webb, I. K.; Garimella, S. V. B.; Hamid, A. M.; Zheng, X.; Norheim, R. V.; Prost, S. A.; Anderson, G. A.; Sandoval, J. A.; Baker, E. S.; Ibrahim, Y. M.; Smith, R. D. Serpentine Ultralong Path with Extended Routing (SUPER) High Resolution Traveling Wave Ion Mobility-MS Using Structures for Lossless Ion Manipulations. *Anal. Chem.* 2017, 89 (8), 4628–4634. https://doi.org/10.1021/acs.analchem.7b00185.
- (22) Wojcik, R.; Nagy, G.; Attah, Isaac. K.; Webb, I. K.; Garimella, S. V. B.; Weitz, K. K.; Hollerbach, A.; Monroe, M. E.; Ligare, M. R.; Nielson, F. F.; Norheim, R. V.; Renslow, R. S.; Metz, T. O.; Ibrahim, Y. M.; Smith, R. D. SLIM Ultrahigh Resolution Ion Mobility Spectrometry Separations of Isotopologues and Isotopomers Reveal Mobility Shifts Due to

- Mass Distribution Changes. *Anal. Chem.* **2019**, *91* (18), 11952–11962. https://doi.org/10.1021/acs.analchem.9b02808.
- (23) Koeniger, S. L.; Merenbloom, S. I.; Valentine, S. J.; Jarrold, M. F.; Udseth, H. R.; Smith, R. D.; Clemmer, D. E. An IMS-IMS Analogue of MS-MS. *Anal. Chem.* 2006, 78 (12), 4161–4174. https://doi.org/10.1021/ac051060w.
- (24) Li, H.; Bendiak, B.; Siems, W. F.; Gang, D. R.; Hill, H. H. Carbohydrate Structure Characterization by Tandem Ion Mobility Mass Spectrometry (IMMS) <sup>2</sup>. *Anal. Chem.* **2013**, 85 (5), 2760–2769. https://doi.org/10.1021/ac303273z.
- (25) Liu, F. C.; Ridgeway, M. E.; Park, M. A.; Bleiholder, C. Tandem Trapped Ion Mobility Spectrometry. *The Analyst* **2018**, *143* (10), 2249–2258. https://doi.org/10.1039/C7AN02054F.
- (26) Eaton, R. M.; Zercher, B.; Wageman, A.; Bush, M. F. A Flexible, Modular Platform for Multidimensional Ion Mobility of Native-like Ions. J. Am. Soc. Mass Spectrom. 2023, DOI:10.1021/jasms.3c00112. https://doi.org/10.1021/jasms.3c00112.
- (27) Benesch, J. L.; Ruotolo, B. T. Mass Spectrometry: Come of Age for Structural and Dynamical Biology. Curr. Opin. Struct. Biol. 2011, 21 (5), 641–649. https://doi.org/10.1016/j.sbi.2011.08.002.
- (28) Wyttenbach, T.; Bowers, M. T. Structural Stability from Solution to the Gas Phase: Native Solution Structure of Ubiquitin Survives Analysis in a Solvent-Free Ion Mobility–Mass Spectrometry Environment. *J. Phys. Chem. B* **2011**, *115* (42), 12266–12275. https://doi.org/10.1021/jp206867a.

- (29) Badman, E. R.; Hoaglund-Hyzer, C. S.; Clemmer, D. E. Monitoring Structural Changes of Proteins in an Ion Trap over ~10–200 Ms: Unfolding Transitions in Cytochrome *c* Ions. *Anal. Chem.* **2001**, *73* (24), 6000–6007. https://doi.org/10.1021/ac010744a.
- (30) Myung, S.; Badman, E. R.; Lee, Y. J.; Clemmer, D. E. Structural Transitions of Electrosprayed Ubiquitin Ions Stored in an Ion Trap over ~10 Ms to 30 s †. *J. Phys. Chem.*A 2002, 106 (42), 9976–9982. https://doi.org/10.1021/jp0206368.
- (31) Eldrid, C.; Ujma, J.; Kalfas, S.; Tomczyk, N.; Giles, K.; Morris, M.; Thalassinos, K. Gas Phase Stability of Protein Ions in a Cyclic Ion Mobility Spectrometry Traveling Wave Device. *Anal. Chem.* 2019, 91 (12), 7554–7561. https://doi.org/10.1021/acs.analchem.8b05641.
- (32) Allen, S. J.; Eaton, R. M.; Bush, M. F. Structural Dynamics of Native-Like Ions in the Gas Phase: Results from Tandem Ion Mobility of Cytochrome *c. Anal. Chem.* **2017**, *89* (14), 7527–7534. https://doi.org/10.1021/acs.analchem.7b01234.
- (33) Poyer, S.; Comby-Zerbino, C.; Choi, C. M.; MacAleese, L.; Deo, C.; Bogliotti, N.; Xie, J.; Salpin, J.-Y.; Dugourd, P.; Chirot, F. Conformational Dynamics in Ion Mobility Data. *Anal. Chem.* **2017**, *89* (7), 4230–4237. https://doi.org/10.1021/acs.analchem.7b00281.
- (34) Le Fèvre, A.; Dugourd, P.; Chirot, F. Exploring Conformational Landscapes Using Trap and Release Tandem Ion Mobility Spectrometry. *Anal. Chem.* **2021**, *93* (9), 4183–4190. https://doi.org/10.1021/acs.analchem.0c04520.
- (35) Mao, Y.; Woenckhaus, J.; Kolafa, J.; Ratner, M. A.; Jarrold, M. F. Thermal Unfolding of Unsolvated Cytochrome c: Experiment and Molecular Dynamics Simulations. *J. Am. Chem. Soc.* 1999, *121* (12), 2712–2721. https://doi.org/10.1021/ja980324b.

- (36) Z. Steinberg, M.; Breuker, K.; Elber, R.; Benny Gerber, R. The Dynamics of Water Evaporation from Partially Solvated Cytochrome c in the Gas Phase. *Phys. Chem. Chem. Phys.* 2007, 9 (33), 4690–4697. https://doi.org/10.1039/B705905A.
- (37) Pacholarz, K. J.; Porrini, M.; Garlish, R. A.; Burnley, R. J.; Taylor, R. J.; Henry, A. J.; Barran, P. E. Dynamics of Intact Immunoglobulin G Explored by Drift-Tube Ion-Mobility Mass Spectrometry and Molecular Modeling. *Angew. Chem. Int. Ed.* **2014**, *53* (30), 7765–7769. https://doi.org/10.1002/anie.201402863.
- (38) Bakhtiari, M.; Konermann, L. Protein Ions Generated by Native Electrospray Ionization: Comparison of Gas Phase, Solution, and Crystal Structures. *J. Phys. Chem. B* **2019**, *123* (8), 1784–1796. https://doi.org/10.1021/acs.jpcb.8b12173.
- (39) Oh, H.; Breuker, K.; Sze, S. K.; Ge, Y.; Carpenter, B. K.; McLafferty, F. W. Secondary and Tertiary Structures of Gaseous Protein Ions Characterized by Electron Capture Dissociation Mass Spectrometry and Photofragment Spectroscopy. *Proc. Natl. Acad. Sci.* 2002, 99 (25), 15863–15868. https://doi.org/10.1073/pnas.212643599.
- (40) Mihalca, R.; Kleinnijenhuis, A. J.; McDonnell, L. A.; Heck, A. J. R.; Heeren, R. M. A. Electron Capture Dissociation at Low Temperatures Reveals Selective Dissociations. *J. Am. Soc. Mass Spectrom.* 2004, 15 (12), 1869–1873. https://doi.org/10.1021/jasms.8b02108.
- (41) McLafferty, F. W.; Guan, Z.; Haupts, U.; Wood, T. D.; Kelleher, N. L. Gaseous Conformational Structures of Cytochrome c. *J. Am. Chem. Soc.* **1998**, *120* (19), 4732–4740. https://doi.org/10.1021/ja9728076.
- (42) Zercher, B. P.; Gozzo, T. A.; Wageman, A.; Bush, M. F. Enhancing the Depth of Analyses with Next-Generation Ion Mobility Experiments. *Annu. Rev. Anal. Chem.* **2023**, *16* (1), annurev-anchem-091522-031329. https://doi.org/10.1146/annurev-anchem-091522-031329.

- (43) Breuker, K.; McLafferty, F. W. Stepwise Evolution of Protein Native Structure with Electrospray into the Gas Phase, 10–12 to 102 s. *Proc. Natl. Acad. Sci.* **2008**, *105* (47), 18145–18152. https://doi.org/10.1073/pnas.0807005105.
- (44) Davidson, K. L.; Oberreit, D. R.; Hogan, C. J.; Bush, M. F. Nonspecific Aggregation in Native Electrokinetic Nanoelectrospray Ionization. *Int. J. Mass Spectrom.* 2017, 420, 35–42. https://doi.org/10.1016/j.ijms.2016.09.013.
- (45) Allen, S. J.; Eaton, R. M.; Bush, M. F. Analysis of Native-Like Ions Using Structures for Lossless Ion Manipulations. *Anal. Chem.* 2016, 88 (18), 9118–9126. https://doi.org/10.1021/acs.analchem.6b02089.
- (46) Eaton, R. M.; Allen, S. J.; Bush, M. F. Principles of Ion Selection, Alignment, and Focusing in Tandem Ion Mobility Implemented Using Structures for Lossless Ion Manipulations (SLIM). *J. Am. Soc. Mass Spectrom.* 2019, 30 (6), 1115–1125. https://doi.org/10.1007/s13361-019-02170-1.
- (47) Allen, S. J.; Giles, K.; Gilbert, T.; Bush, M. F. Ion Mobility Mass Spectrometry of Peptide, Protein, and Protein Complex Ions Using a Radio-Frequency Confining Drift Cell. *Analyst* 2016, 141 (3), 884–891. https://doi.org/10.1039/C5AN02107C.
- (48) Hong, S.; Bush, M. F. Collision-Induced Unfolding Is Sensitive to the Polarity of Proteins and Protein Complexes. J. Am. Soc. Mass Spectrom. 2019, 30 (11), 2430–2437. https://doi.org/10.1007/s13361-019-02326-z.
- (49) Harris, C. R.; Millman, K. J.; Van Der Walt, S. J.; Gommers, R.; Virtanen, P.; Cournapeau, D.; Wieser, E.; Taylor, J.; Berg, S.; Smith, N. J.; Kern, R.; Picus, M.; Hoyer, S.; Van Kerkwijk, M. H.; Brett, M.; Haldane, A.; Del Río, J. F.; Wiebe, M.; Peterson, P.; Gérard-Marchant, P.; Sheppard, K.; Reddy, T.; Weckesser, W.; Abbasi, H.; Gohlke, C.; Oliphant,

- T. E. Array Programming with NumPy. *Nature* **2020**, *585* (7825), 357–362. https://doi.org/10.1038/s41586-020-2649-2.
- (50) The Astropy Collaboration; Price-Whelan, A. M.; Lim, P. L.; Earl, N.; Starkman, N.; Bradley, L.; Shupe, D. L.; Patil, A. A.; Corrales, L.; Brasseur, C. E.; Nöthe, M.; Donath, A.; Tollerud, E.; Morris, B. M.; Ginsburg, A.; Vaher, E.; Weaver, B. A.; Tocknell, J.; Jamieson, W.; van Kerkwijk, M. H.; Robitaille, T. P.; Merry, B.; Bachetti, M.; Günther, H. M.; Aldcroft, T. L.; Alvarado-Montes, J. A.; Archibald, A. M.; Bódi, A.; Bapat, S.; Barentsen, G.; Bazán, J.; Biswas, M.; Boquien, M.; Burke, D. J.; Cara, D.; Cara, M.; Conroy, K. E.; Conseil, S.; Craig, M. W.; Cross, R. M.; Cruz, K. L.; D'Eugenio, F.; Dencheva, N.; Devillepoix, H. A. R.; Dietrich, J. P.; Eigenbrot, A. D.; Erben, T.; Ferreira, L.; Foreman-Mackey, D.; Fox, R.; Freij, N.; Garg, S.; Geda, R.; Glattly, L.; Gondhalekar, Y.; Gordon, K. D.; Grant, D.; Greenfield, P.; Groener, A. M.; Guest, S.; Gurovich, S.; Handberg, R.; Hart, A.; Hatfield-Dodds, Z.; Homeier, D.; Hosseinzadeh, G.; Jenness, T.; Jones, C. K.; Joseph, P.; Kalmbach, J. B.; Karamehmetoglu, E.; Kałuszyński, M.; Kelley, M. S. P.; Kern, N.; Kerzendorf, W. E.; Koch, E. W.; Kulumani, S.; Lee, A.; Ly, C.; Ma, Z.; MacBride, C.; Maljaars, J. M.; Muna, D.; Murphy, N. A.; Norman, H.; O'Steen, R.; Oman, K. A.; Pacifici, C.; Pascual, S.; Pascual-Granado, J.; Patil, R. R.; Perren, G. I.; Pickering, T. E.; Rastogi, T.; Roulston, B. R.; Ryan, D. F.; Rykoff, E. S.; Sabater, J.; Sakurikar, P.; Salgado, J.; Sanghi, A.; Saunders, N.; Savchenko, V.; Schwardt, L.; Seifert-Eckert, M.; Shih, A. Y.; Jain, A. S.; Shukla, G.; Sick, J.; Simpson, C.; Singanamalla, S.; Singer, L. P.; Singhal, J.; Sinha, M.; Sipőcz, B. M.; Spitler, L. R.; Stansby, D.; Streicher, O.; Šumak, J.; Swinbank, J. D.; Taranu, D. S.; Tewary, N.; Tremblay, G. R.; de Val-Borro, M.; Van Kooten, S. J.; Vasović, Z.; Verma, S.; Cardoso, J. V. de M.; Williams, P. K. G.; Wilson, T.

- J.; Winkel, B.; Wood-Vasey, W. M.; Xue, R.; Yoachim, P.; ZHANG, C.; Zonca, A. The Astropy Project: Sustaining and Growing a Community-Oriented Open-Source Project and the Latest Major Release (v5.0) of the Core Package. **2022**. https://doi.org/10.48550/ARXIV.2206.14220.
- (51) Allen, S. J.; Bush, M. F. Radio-Frequency (RF) Confinement in Ion Mobility Mass Spectrometry: Apparent Mobilities and Effective Temperatures. *J. Am. Soc. Mass Spectrom.* **2016**, *27*, 2054–2063. https://doi.org/10.1007/s13361-016-1479-9.
- (52) Bush, M. F.; Hall, Z.; Giles, K.; Hoyes, J.; Robinson, C. V.; Ruotolo, B. T. Collision Cross Sections of Proteins and Their Complexes: A Calibration Framework and Database for Gas-Phase Structural Biology. *Anal. Chem.* 2010, 82 (22), 9557–9565. https://doi.org/10.1021/ac1022953.
- (53) Freeke, J.; Bush, M. F.; Robinson, C. V.; Ruotolo, B. T. Gas-Phase Protein Assemblies:

  Unfolding Landscapes and Preserving Native-like Structures Using Noncovalent Adducts.

  Chem. Phys. Lett. 2012, 524, 1–9. https://doi.org/10.1016/j.cplett.2011.11.014.
- (54) Dixit, S. M.; Polasky, D. A.; Ruotolo, B. T. Collision Induced Unfolding of Isolated Proteins in the Gas Phase: Past, Present, and Future. *Curr. Opin. Chem. Biol.* 2018, 42, 93–100. https://doi.org/10.1016/j.cbpa.2017.11.010.
- (55) Pierson, N. A.; Valentine, S. J.; Clemmer, D. E. Evidence for a Quasi-Equilibrium Distribution of States for Bradykinin [M + 3H]3+ Ions in the Gas Phase. *J. Phys. Chem. B* 2010, 114 (23), 7777–7783. https://doi.org/10.1021/jp102478k.
- (56) Devine, P. W. A.; Fisher, H. C.; Calabrese, A. N.; Whelan, F.; Higazi, D. R.; Potts, J. R.; Lowe, D. C.; Radford, S. E.; Ashcroft, A. E. Investigating the Structural Compaction of

- Biomolecules Upon Transition to the Gas-Phase Using ESI-TWIMS-MS. *J. Am. Soc. Mass Spectrom.* **2017**, *28* (9), 1855–1862. https://doi.org/10.1007/s13361-017-1689-9.
- (57) Hernandez-Alba, O.; Wagner-Rousset, E.; Beck, A.; Cianférani, S. Native Mass Spectrometry, Ion Mobility, and Collision-Induced Unfolding for Conformational Characterization of IgG4 Monoclonal Antibodies. *Anal. Chem.* 2018, 90 (15), 8865–8872. https://doi.org/10.1021/acs.analchem.8b00912.
- (58) Hansen, K.; Lau, A. M.; Giles, K.; McDonnell, J. M.; Struwe, W. B.; Sutton, B. J.; Politis, A. A Mass-Spectrometry-Based Modelling Workflow for Accurate Prediction of IgG Antibody Conformations in the Gas Phase. *Angew. Chem. Int. Ed.* 2018, 57 (52), 17194–17199. https://doi.org/10.1002/anie.201812018.
- (59) Tian, Y.; Han, L.; Buckner, A. C.; Ruotolo, B. T. Collision Induced Unfolding of Intact Antibodies: Rapid Characterization of Disulfide Bonding Patterns, Glycosylation, and Structures. *Anal. Chem.* 2015, 87 (22), 11509–11515. https://doi.org/10.1021/acs.analchem.5b03291.
- (60) Morsa, D.; Gabelica, V.; De Pauw, E. Effective Temperature of Ions in Traveling Wave Ion Mobility Spectrometry. *Anal. Chem.* 2011, 83 (14), 5775–5782. https://doi.org/10.1021/ac201509p.
- (61) Merenbloom, S. I.; Flick, T. G.; Williams, E. R. How Hot Are Your Ions in TWAVE Ion Mobility Spectrometry? J. Am. Soc. Mass Spectrom. 2012, 23 (3), 553–562. https://doi.org/10.1007/s13361-011-0313-7.
- (62) Morsa, D.; Hanozin, E.; Eppe, G.; Quinton, L.; Gabelica, V.; Pauw, E. D. Effective Temperature and Structural Rearrangement in Trapped Ion Mobility Spectrometry. *Anal. Chem.* 2020, 92 (6), 4573–4582. https://doi.org/10.1021/acs.analchem.9b05850.

**Table 1.** Results from Kinetic Modeling $^a$ 

Ion	$\Omega_A$ / nm <sup>2</sup>	$\Omega_B$ / nm <sup>2</sup>	Rate Constant / s <sup>-1</sup>
7+ cytochrome <i>c</i>	$15.78 \pm 0.03$	$16.56 \pm 0.07$	$0.28 \pm 0.07$
5+ ubiquitin	$11.97 \pm 0.02$	$12.31 \pm 0.02$	$0.91 \pm 0.20$
6+ ubiquitin	$12.54 \pm 0.03$	$14.28 \pm 0.03$	$0.84 \pm 0.05$

<sup>&</sup>lt;sup>a</sup> These parameters and the associated methodology are described in the *Methods* section. The intervals span  $\pm 1$  standard deviation.

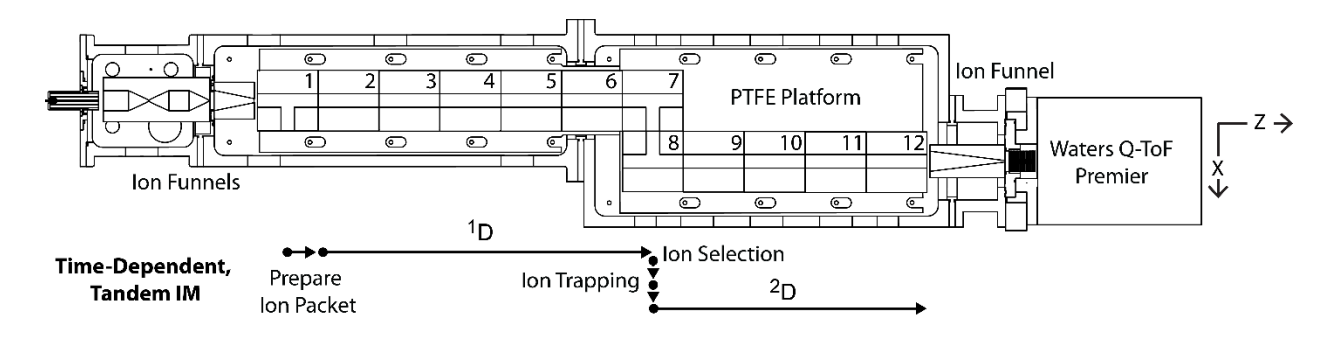


**Figure 1**. Schematic of the 12-module array used for these experiments.<sup>26</sup> Ions generated at atmospheric pressure pass through a stainless-steel capillary heated to 80 °C (*far left*), a hourglass ion funnel, and a rectangular ion funnel prior to the array of 12 modules. Ions are transported through these modules using electrostatic fields, not traveling waves, and data analysis is like that of drift tubes. The first module (<sup>1</sup>M), <sup>7</sup>M, and <sup>8</sup>M are tee modules, whereas the remaining modules are linear modules. Finally, ions pass through a circular ion funnel that interfaces with the mass analyzer. Ion packets are prepared on the <sup>1</sup>M, then separated in the first dimension of IM (<sup>1</sup>D) prior to selection at the <sup>7</sup>M. Ions are then trapped at the interface between the <sup>7</sup>M and <sup>8</sup>M for varying periods of time before separation in a second dimension of IM (<sup>2</sup>D) prior to mass analysis.

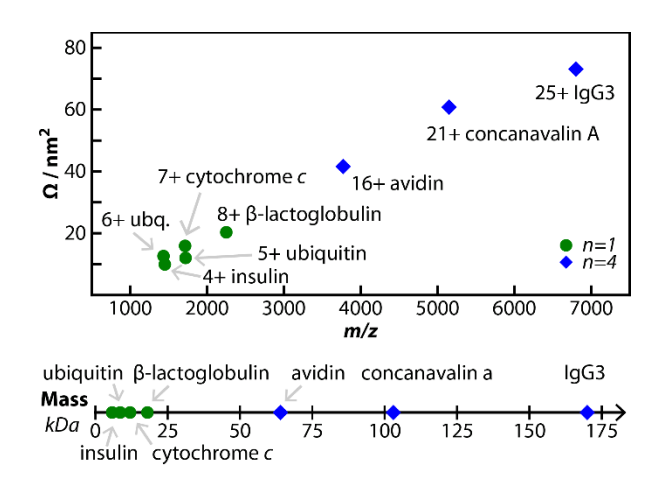


Figure 2. The properties of the native-like ions analyzed in these time-dependent, tandem IM experiments. (Top) Reported collision cross sections in nitrogen ( $\Omega$ ) of the selected charge states versus their m/z values; n represents the oligomeric state of the protein. Avidin and concanavalin A are homotetramers, whereas IgG3 is composed of two heavy and two light peptide chains that are connected through covalent and noncovalent interactions. (Bottom) The proteins analyzed in this study plotted by their mass.

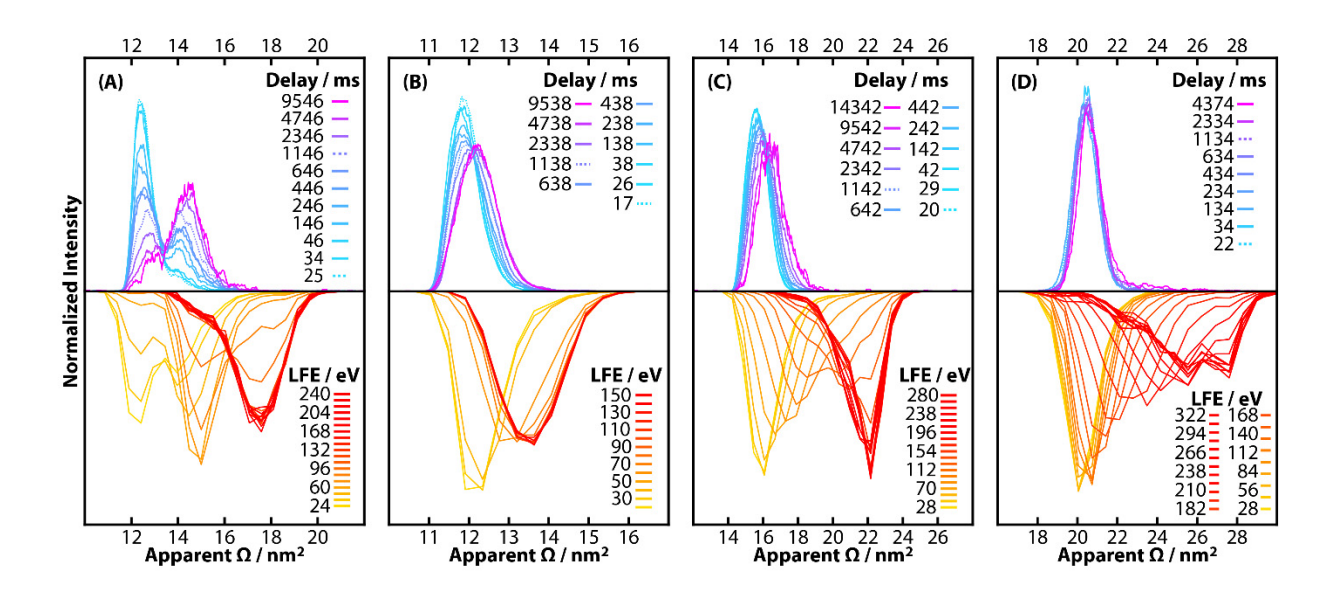


Figure 3. Apparent  $\Omega$  distributions determined from time-dependent (positive intensity, cool color scheme) and energy-dependent (negative intensity, hot color scheme) experiments for (A) 6+ ubiquitin, (B) 5+ ubiquitin, (C) 7+ cytochrome c, and (D) 8+ β-lactoglobulin. In the panels for the time-dependent experiments (*top row*), the delay time describes the time between ion selection and ion mobility analysis in the  $^2$ D. Selected traces are plotted using dotted lines (as indicated in the key) to aid in visualization. In the panels for the energy-dependent experiments (*bottom row*), results are plotted in terms of the laboratory-frame energy (LFE) for each experiment. 4+ insulin was characterized in both time-dependent and energy-dependent experiments; apparent  $\Omega$  distributions were independent of both time and energy (Figure S1).

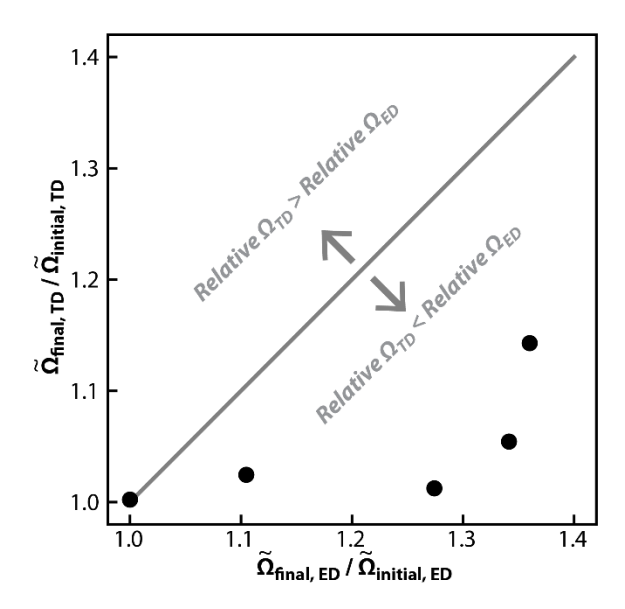
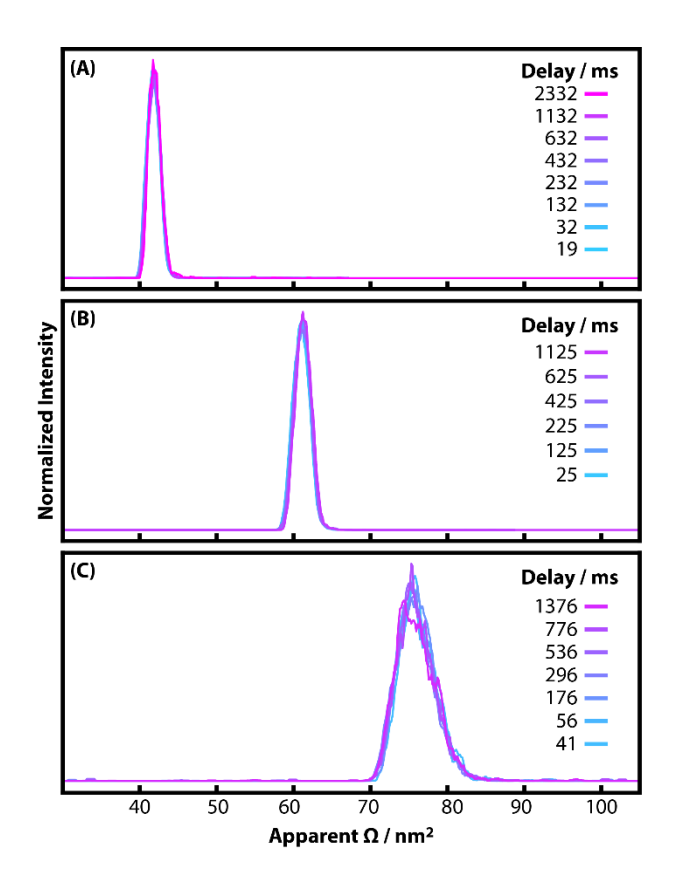


Figure 4. Relative  $\Omega$  values from time-dependent (TD) experiments as a function of those values from energy-dependent (ED) experiments for each monomeric protein ion studied. A relative  $\Omega$  value is the ratio of the median  $\Omega$  ( $\widetilde{\Omega}$ ) for the ion populations that experienced the longest delay time or the highest laboratory-frame energies ("final") relative to that for those that experienced shortest delay time or the lowest laboratory-frame energies ("initial"). From left to right, the markers correspond to 4+ insulin, 5+ ubiquitin, 8+ β-lactoglobulin, 7+ cytochrome c, and 6+ ubiquitin. The line has a slope of 1.



**Figure 5.** Apparent  $\Omega$  distributions as a function of delay time for 16+ avidin (A), 21+ concanavalin A (B), 25+ IgG3 (C). Each distribution is the average of three replicate measurements and is normalized by area.

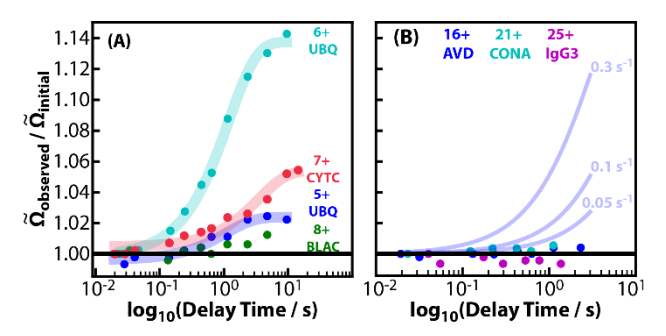


Figure 6. Relative  $\widetilde{\Omega}$  values as a function of the delay time for monomeric (A) and multimeric (B) proteins. Transparent lines are from kinetic modeling of the data; the methodology is described in the *Supporting Information*. For monomeric proteins, kinetic models were fit to experimental data to determine rate constants (Table S3), whereas the models in Panel B describe transitions from the observed  $\widetilde{\Omega}_{initial}$  of 16+ avidin to a final extended state<sup>48</sup> at selected rate constant.

# For Table of Contents Only

